A discrete-continuum coupled finite element model to simulate all failure modes in fibre reinforced concrete

***H. Zhang, Y.J. Huang, †Z.J. Yang, S.L. Xu**

College of Civil Engineering and Architecture, Zhejiang University, 310058, China.

*Presenting author: huizhangzju@zju.edu.cn
†Corresponding author: zhjyang@zju.edu.cn

Abstract

Fibre reinforced concrete (FRC) exhibits complicated failure modes such as fibre breakage, mortar cracking and spalling, fibre-mortar interfacial debonding, depending on many material properties, geometric dimensions and loading conditions. Most existing numerical models are unable to reproduce the above failure modes that may occur simultaneously or sequentially, mainly due to the difficulty in generating finite element meshes with a large number of randomly-oriented fibres. Herein we develop a discrete-continuum coupled finite element model for FRC capable of effectively simulating all the major failure modes. The continuum damage-plasticity model is used to simulate damage and fracture behaviour of the mortar, while debonding of fibre-mortar interfaces is modelled by nonlinear cohesive interfacial elements. Unique techniques are identified to generate conforming meshes between fibres and the surrounding mortar so that randomly-oriented fibres are easily modelled. The model is validated by simulating single fibre pullout tests with different inclination angles and direct tensile tests of multiple randomly-distributed fibres.

Keywords: Fibre reinforced concrete; Cohesive crack model; Damaged plasticity model; Damage and fracture; Interfacial debonding; Finite element model

Introduction

Fibre reinforced concrete (FRC) is a cementitious composite material making use of fibres' high tensile strength and bridging capability to compensate the low fracture resistance of traditional concrete. At micro/meso-scales, an FRC material is a composite comprising mortar matrix, reinforcing fibres, fibre-mortar interfaces and pores. Its mechanical properties and failure behaviour are very complicated, depending on many factors such as the strength, stiffness and volume/weight fractions of the constituents, the length, shape and distribution of fibres, the size, number and distribution of pores, and inter-phasic interactions such as bond-slip between fibres and mortar. Depending on the relative values of these factors, various failure modes with distinguished characteristics can take place, such as fibre breakage, mortar cracking, crushing and spalling, and fibre-mortar interfacial debonding.

Although many finite element (FE) models with multiple fibres have so far been developed for numerical homogenization of elastic properties, either based on computer-generated fibres with random orientations [1] or more recently, converted directly from realistic images, such as from X-ray computed tomography scanning [2], nonlinear FE models with multiple fibres are still rare. For example, Cunha et al. [3] used the smeared crack model and Yu et al. [4] assumed elastic behaviour for the matrix and both modelled beam-bending tests with a single cohesive crack in the middle. The fibre-matrix interaction was indirectly modelled by equivalent tensile stress-strain constitutive laws of fibres transformed from load-slip curves of the single fibre pullout tests (SFPTs). However, the equivalent transformation remains empirical and arguable. In particular, for the fibre embedded length, which is a key parameter, Cunha et al. [3] used a quarter of fibre length and Yu et al. [4] used the total fibre length assuming uniform stress distribution along the fibre. It is also difficult to interpret the resultant stress in a fibre, as it mixes the effects of elongation in itself and bond-slip on the fibre-matrix interface.

This study is aimed at developing an innovative, easy-to-implement, discrete-continuum coupled finite element model, which is capable of simulating all the possible failure mechanisms in FRC with a large number of fibres at the micro/meso-scales. In this model, all the material phases, i.e., the fibres, the matrix and the fibre-matrix interfaces are individually and explicitly represented. All the major failure mechanisms at micro/meso-scales can be simulated by the proposed model, depending on the relative material properties of different phases. Moreover, the ambiguous assumptions and reliance on the load-slip curves from macro-scale SFPTs, required by many existing models for interfacial bond-slip simulation, are now not needed. As realistic constitutive laws are assigned for each phase, all the results have clear physical interpretation, and parametric studies can be carried out to optimise the key parameters at the material level.

Methodology

Mesh Generation

Fibres are randomly distributed in the domain. Random numbers are generated and used to define the first fibre's centre point and its orientation. The two end points of the fibre are then calculated as the fibre length is known. The fibre will be shortened if it intersects with the domain boundary. The next fibre is then generated in the same way until the given volume fraction of fibres is reached.

A two-step scheme is devised to generate the mesh. In the first step (see Fig. 1a), all the fibres are set as Part A and the matrix as Part B in ABAQUS. A Boolean operation is then performed to merge the fibres into the matrix, which makes the fibre geometries as boundaries of the matrix so that the fibres share the same nodes as the matrix after meshing (i.e., conforming). In the second step, zero-thickness cohesive elements (COH2D4 in ABAQUS) are inserted between pairs of fibre and matrix elements to model the fibre-matrix interface, using a simple MATLAB code (Fig. 1b). The cohesive elements are arranged in a unique way that both the fibres and interfaces are deformed in the plane. Fig. 1c shows a special case when two fibres intersect with each other. At the intersection, three nodes with the same coordinates are used, i.e., N1 of fibre 1, N2 of fibre 2 and N3 of the matrix.

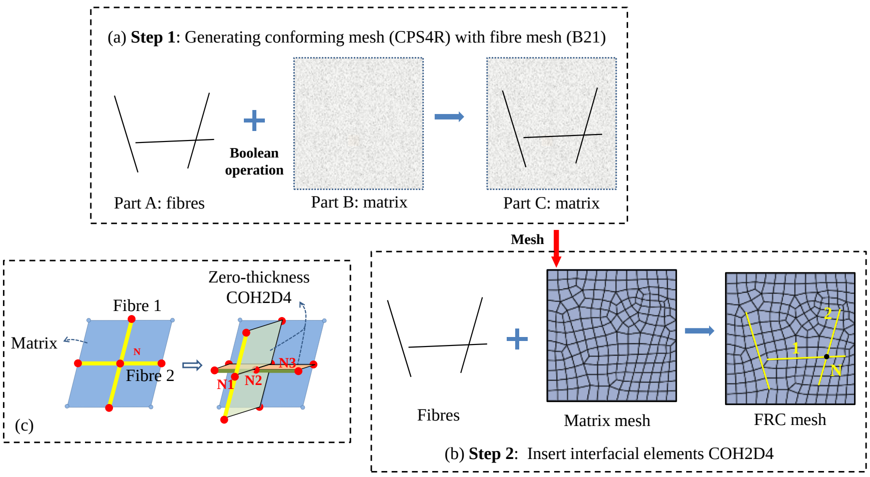

Figure 1. A two-step scheme to generate the FRC mesh

Constitutive Laws

The fibres are modelled using two-noded Timoshenko beam elements (B21 in ABAQUS) with elastic-plastic stress-strain laws with yielding strain hardening and rupture. The bending stiffness and tensile stiffness are calculated based on the cross-sectional area of the fibre as an input.

The mortar matrix is described by the concrete damage plasticity (CDP) model in ABAQUS. The CDP model has been widely used in static and dynamic damage and fracture modelling of concrete [5]-[7]. It has also been used to model the mortar matrix [8].This study assumes linear-elastic pre-peak compressive and tensile stress-strain relations for the matrix. The post-peak softening response in compression (σ_c-ε_c) is described using [9] and the tensile traction (σ_t)-crack opening displacement (w) by [10].

The fibre-matrix interfacial behaviour is simulated by zero-thickness cohesive elements (COH2D4 in ABAQUS) which assumes that there exist a normal traction t_n and a tangential traction (shear cohesion) t_s across the crack surfaces. The tractions decrease monotonically as functions of the corresponding relative displacements of the crack surfaces. In this study, the max normal traction t_n^0 is assumed as 10 times the max shear traction t_s^0 so that the interfacial shear slip governing debonding is dominant. Typical linear and exponential softening curves for t_s-δ_s can be used. The resilient feature of cohesive elements is that its formulation is based on the damage mechanics framework, within which the stiffness k_s upon unloading and reloading is degraded as δ_s increases, due to irreversibly progressive damage. The damage is characterized by a non-negative scalar index D representing the overall damage of the interface caused by all physical mechanisms. Apart from the damage evolution laws, a damage initiation law is also needed. A maximum stress law is used in this study, i.e., when t_s reaches t_s^0, D develops and the tangential shear stiffness k_s starts to degrade.

Benchmark: Modelling of Single Fibre Pullout Tests (SFPTs)

The SFPTs with three fibre inclination angles ($\theta = 0°$, $30°$ and $60°$) performed by [11] were simulated first using the develop methodology as a benchmark. The fibre has diameter $d_f = 0.5$ mm and embedment length $L_e = 10$ mm. The geometry, dimensions and boundary conditions are shown in Fig. 2. The fibre free end is constrained vertically and can only move horizontally. This is to simulate the stress condition of a fibre crossing a crack. The material properties are given in Table 1. The fracture energy for the matrix is $G_f = 0.04$ N/mm for all the simulations in this study. According to the experiment, the fibre-matrix interfacial bonding strength is $t_s^0 = P_{max}/(\pi d_f l_f) = 3.3$ MPa, where the maximum pullout force P_{max} was estimated to be 52 N after averaging experimental results for $\theta = 0°$. The exponential damage evolution law was used for the cohesive elements.

For all the simulations in this study, the ABAQUS/Explicit solver is employed with total time 0.01 s to ensure the quasi-static loading condition for all the simulations in this paper.

Table 1. Material parameters for the SFPTs

	E (GPa)	ν –	ρ (kg/m^3)	f_c (MPa)	f_t (MPa)	f_y (MPa)	f_b (MPa)	ε_b –	L_f (mm)	D_f (mm)	t_s^0 (MPa)
Matrix	27	0.2	2100	36.5	3.0	–	–	–	–	–	–

Fibre	200	0.33	7800	–	–	635	847	0.1	10	0.5	–
Interface	10	0.3	2100	–	–	–	–	–	–		3.3

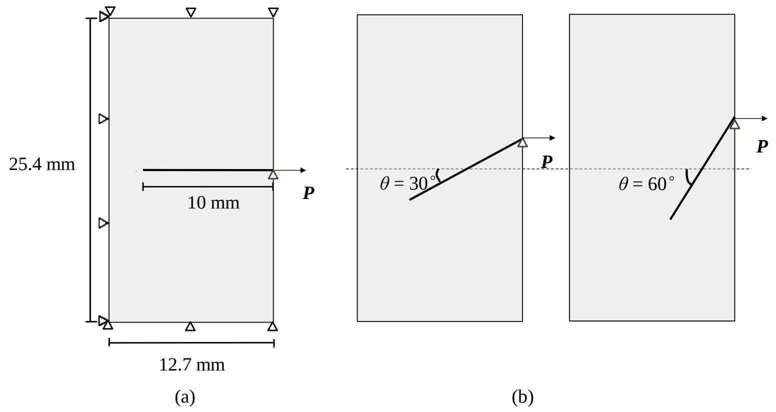

Figure 2. (a) In-plane dimensions and boundary conditions in the pullout tests; (b) fibres inclination angles of 30° and 60°

A mesh convergence study was carried out first for the specimen with θ = 30° using three meshes as shown in Fig. 3. The three meshes have 25, 50 and 75 divisions in the fibre across a zone with width of 4 mm, 8 mm and 12 mm, respectively. The predicted pullout force-slip (*P-s*) curves are plotted in Fig. 4. It can be seen that virtually identical results were obtained from the medium and fine meshes. Therefore, the medium mesh was used after considering the balance between efficiency and accuracy.

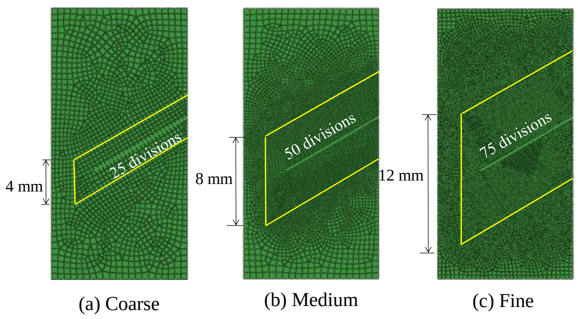

Figure 3. Three meshes for sensitivity study

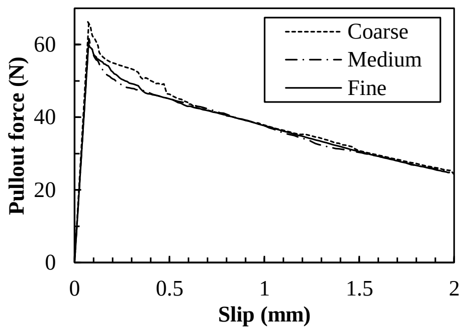

Figure 4. The pullout force slip (*P-s*) relations from three meshes (θ = 30°)

The predicted P-s curves are compared with the experimental data with good agreement, as shown in Figs. 5a, 5b and 5c for θ = 0°, 30° and 60°, respectively.

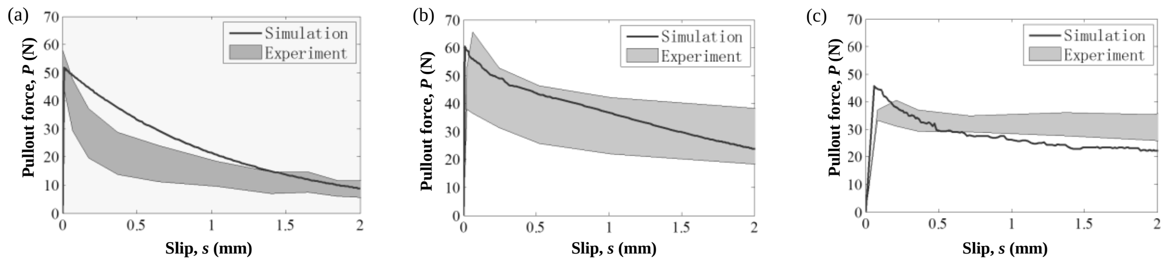

Figure 5. Pullout force-slip (P-s) relations: (a) $\theta = 0°$; (b) $\theta = 30°$; (c) $\theta = 60°$

Modelling Direct Tensile Tests of UHPFRC Specimens with Multi-Fibres

Direct tensile tests of UHPFRC specimens are simulated herein against the experiment of Yoo et al. [12] to demonstrate the capability of modelling multiple cracks. The material parameters listed in Table 2 are from the experiment. Ten random samples with V_f = 2.0% are modelled and one of them is shown in Fig. 6a with the dimensions and boundary conditions. Fig. 6b shows a local mesh in this sample with typical elemental size 0.5 mm.

Table 2. Material parameters for the UHPFRC specimen

	E (GPa)	ν –	ρ (kg/m^3)	f_c (MPa)	f_t (MPa)	f_y (MPa)	f_b (MPa)	ε_b –	L_f (mm)	D_f (mm)	t_s^0 (MPa)
Matrix	27	0.2	2100	150	9	–	–	–	–	–	–
Fibre	200	0.33	7800	–	–	2500	2800	0.1	13	0.2	–
Interface	10	0.3	2100	–	–	–	–	–	–		7.5

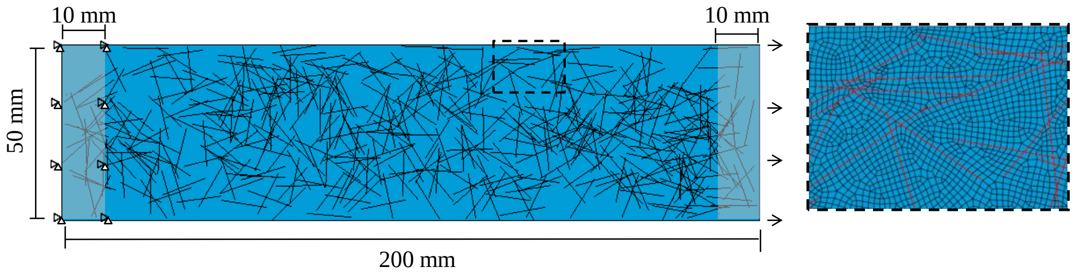

(a) (b)

Figure 6. Direct tension of a UHPFRC specimen

The simulated stress-displacement (σ-d) curves from the ten samples are compared with the experimental data in Fig. 7. Excellent agreement can be seen. Again the scatter among the simulation results reflects the different fibre distribution in different samples. The damage and fracture process for one sample is illustrated in Fig. 8 at a few displacements. It can be seen that damage initiates mostly in the matrix areas with fewer fibres before the peak load (Fig. 8a). As the displacement increases, these damaged areas gradually develop into many distributed, mostly parallel cracks near the peak load (Fig. 8b), which is typical for the UHPFRC due to fibre bridging. A very complicated damage and crack pattern follows with strong interaction with fibre-matrix interfacial debonding (Fig. 8c). Eventually, the model fails with one or a few localized major cracks (Fig. 8d).

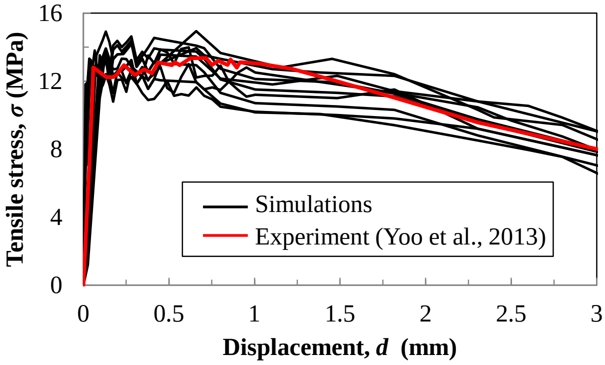

Figure 7. Tensile stress-displacement (*σ*-*d*) curves of SFRC under uniaxial tension for different samples comparing to the experiment result

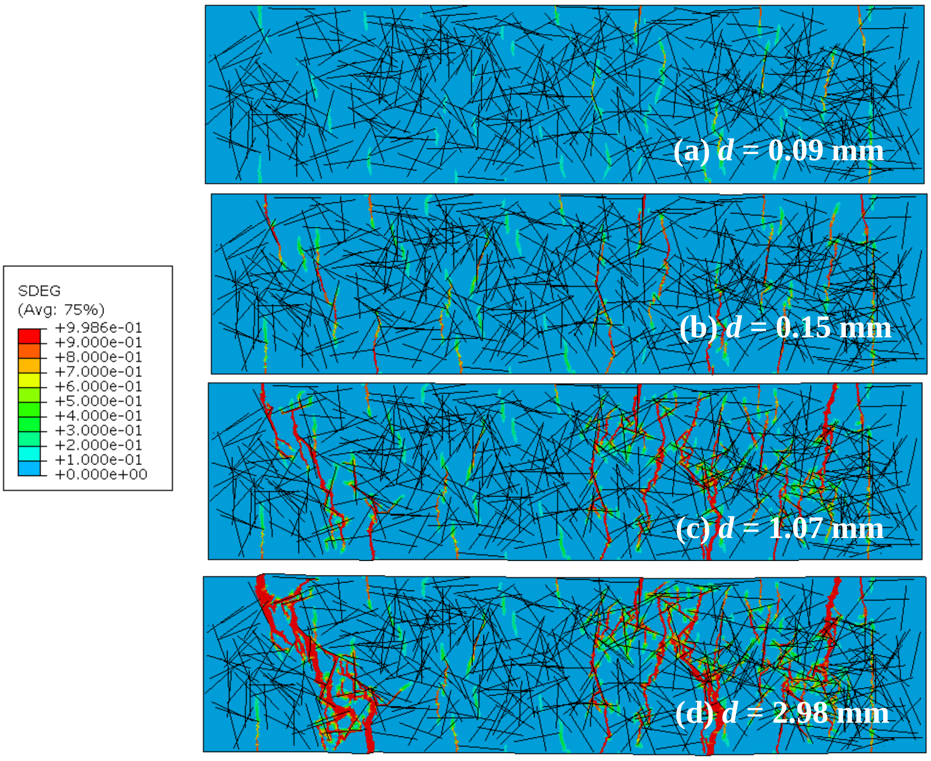

Figure 8. Cracking process of a UHPFRC sample

A cut-off view of Fig. 8d is further shown in Fig. 9 with matrix elements with DAMAGET ≥ 0.9 removed, highlighting the mechanisms such as fibre pullout (A), fibre bending (B, C) and fibre yielding (C) as well as matrix damage due to the snubbing effect of inclined fibres (A, B, C).

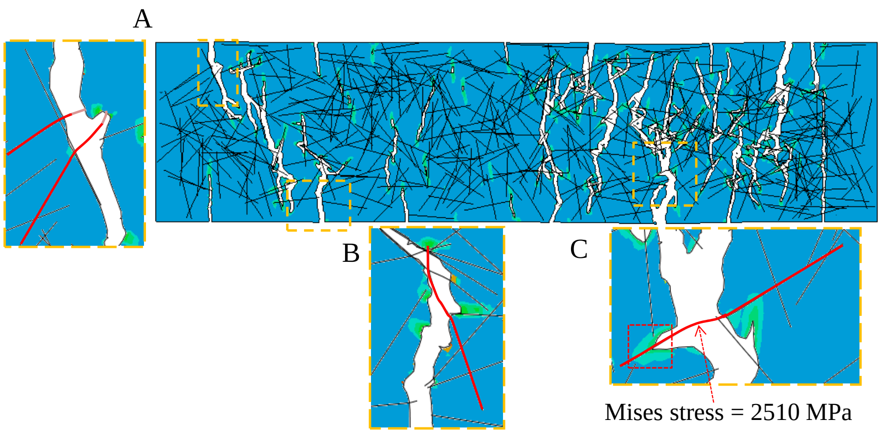

Figure 9. Cut-off view of the fractured sample in Fig. 8d

The failure patterns of two other samples are shown in Fig. 10. It can be seen that the very complicated multi-cracking behaviour of UHPFRC are well captured by the models. The very different failure patterns due to random distribution of fibres are also reported in the experiment [12].

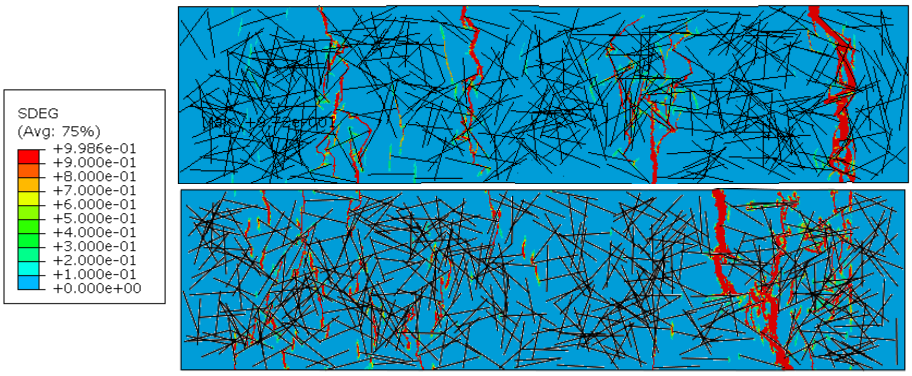

Figure 10. Failure patterns of two other UHPFRC samples

Conclusions

This study has developed an easy-to-implement but effective discrete-continuum coupled modelling approach to simulate complicated nonlinear damage and fracture behaviour of fibre reinforced concrete at the meso-scale. It has been demonstrated that, thanks to explicit, direct modelling of fibres, matrix and fibre-matrix interfaces, this approach is capable of effectively simulating all the possible failure mechanisms that may occur simultaneously or sequentially in one specimen, including fibre pullout, yielding and rupture, interfacial debonding, and matrix cracking and spalling (snubbing effect). This capability allows for parametric studies of key material and geometric factors such as the interfacial bonding strength, matrix tensile strength, fibre volume fraction, and fibre embedment length, so that “optimal” FRC materials can be designed at meso-scale for desired mechanical properties with minimum material cost by optimising these factors.

Acknowledgements

This research is funded by Zhejiang Provincial Natural Science Foundation of China (No. LR14E080002), the Fundamental Research Funds for the Central Universities (No. 172210173) and the National Natural Science Foundation of China (No. 51378462).

References

[1] Gal, E., and Kryvoruk, R. (2011) Meso-scale analysis of FRC using a two-step homogenization approach. *Computers & Structures* **89**, 921-929.

[2] Qsymah, A., Sharma, R., Yang, Z., Margetts, L., and Mummery, P. (2017) Micro X-ray computed tomography image-based two-scale homogenisation of ultra high performance fibre reinforced concrete. *Construction & Building Materials* **130**, 230-240.

[3] Cunha, V. M., Barros, J. A., and Sena-Cruz, J. M. (2012) A finite element model with discrete embedded elements for fibre reinforced composites. *Computers & Structures* **94**, 22-33.

[4] Yu, R. C., Cifuentes, H., Rivero, I., Ruiz, G., and Zhang, X. (2016) Dynamic fracture behaviour in fibre-reinforced cementitious composites. *Journal of the Mechanics & Physics of Solids* **93**, 135-152.

[5] Chen, G. M., Teng, J. G., Chen, J. F., and Rosenboom, O. A. (2010) Interaction between steel stirrups and shear-strengthening FRP strips in RC beams. *Journal of Composites for Construction* **14**, 498-509.

[6] Chen, G. M., Chen, J. F., and Teng, J. G. (2012) On the finite element modelling of RC beams shear-strengthened with FRP. *Construction & Building Materials* **32**, 13-26.

[7] Xu, N., Xu, B., Zeng, X., Jiang, Z., and Chen, J. M. (2010) Dynamic load-displacement behavior of RC shear walls under different loading rates: tests and simulations. *Advanced Materials Research* **163**, 1780-1785.

[8] Huang, Y. J., Yang, Z. J., Chen, X. W., and Liu, G. H. (2016). Monte Carlo simulations of meso-scale dynamic compressive behavior of concrete based on X-ray computed tomography images. *International Journal of Impact Engineering* **97**, 102-115.

[9] Guo, Z.H. Concrete strength and constitutive relation: principle and application. Beijing: China Architecture and Building Press; 2004 ISBN: 9787112062782

[10] Hordijk, D. A. (1992) Tensile and tensile fatigue behaviour of concrete; experiments, modelling and analyses. *Heron* **37,** 1–79.

[11] Leung, C. K. Y., and Shapiro, N. (1999) Optimal steel fiber strength for reinforcement of cementitious materials. *Journal of Materials in Civil Engineering* **11**, 116-123.

[12] Yoo, D. Y., Kang, S. T., Lee, J. H., and Yoon, Y. S. (2013) Effect of shrinkage reducing admixture on tensile and flexural behaviors of uhpfrc considering fiber distribution characteristics. *Cement & Concrete Research* **54**, 180–190.